True Liquefaction Triggering Curve

Sneha Upadhyaya, S.M.ASCE[1]; Russell A. Green, F.ASCE[2]; Adrian Rodriguez-Marek, M.ASCE[3]; and Brett W. Maurer, M.ASCE[4]

Abstract: Current simplified models for predicting liquefaction triggering and manifestation do not account for the mechanisms of liquefaction triggering and surface manifestation in a consistent and sufficient manner. Specifically, an artifact of the way simplified triggering curves have traditionally been developed is that they inherently include some factors that influence surface manifestations, particularly for medium-dense to dense soils. As a result, using the simplified triggering curves in conjunction with the manifestation models results in the double-counting, omission, or general obscuration of distinct factors that influence triggering and manifestation. Accordingly, the objective of this paper is to develop a framework for deriving a true simplified liquefaction triggering model consistent with a defined manifestation model, such that factors influential to triggering and manifestation are handled more rationally and consistently. Operating in conjunction with the LSN_{ish} manifestation model, the performance of the true triggering curve is compared with an existing, popular triggering curve using a set of 50 global case histories; the results are favorable for the proposed framework. Furthermore, the ability of the true liquefaction model to be used in conjunction with manifestation models that account for complex free-field soil profile stratigraphies or developed sites is a significant advantage over traditionally developed triggering models. **DOI: 10.1061/JGGEFK.GTENG-11126.**

Introduction

Soil liquefaction is a leading cause of ground failure during earthquakes, resulting in significant damage to infrastructure around the world. For example, the M_w7.1 September 2010 Darfield earthquake, M_w6.2 February 2011 Christchurch earthquake, and M_w5.7 February 2016 Valentine's Day earthquake, collectively referred to herein as the Canterbury earthquakes (CE), induced widespread liquefaction causing extensive damage to infrastructure and residential buildings throughout the city of Christchurch and its surroundings (e.g., Allen et al. 2010; Cubrinovski et al. 2011; Green et al. 2011, 2014; Maurer et al. 2014; van Ballegooy et al. 2014b). These, along with other recent events (e.g., the 2010 Maule earthquake in Chile, and the 2011 Tohoku earthquake in Japan) highlight the need to accurately predict the occurrence and damage potential of liquefaction. The objective of this paper is to develop a framework for deriving a stress-based liquefaction triggering model consistent with a defined manifestation model, such that factors influential to triggering and manifestation are handled more rationally, consistently, and transparently. This work is motivated by the fact that nearly all field observations available to develop triggering models are made at the ground surface, rather than in discrete strata at specific depths. The interpretation of liquefaction manifestations observed at the ground surface, or the lack thereof, thus presents an inverse problem since liquefaction could occur in various strata, at various depths, and to varying severities but result in a surface manifestation that is perceptibly the same. As a result, the development of a triggering model inherently requires accounting for factors influencing surficial manifestations. However, to date, this has largely been done using judgment, and because of the inherent inconsistency of this approach, it is difficult to use existing triggering models in a manner consistent with their respective developments. This inconsistency, its potential consequences, and the solution proposed herein are further developed in the following.

The stress-based simplified model is the most widely-used approach for predicting liquefaction triggering. The earliest of these models was proposed independently by Whitman (1971) and Seed and Idriss (1971) and has continually been updated as additional field case histories are compiled and as numerical and laboratory results improve the understanding of liquefaction phenomena. However, the fundamental approach to developing triggering models has largely remained the same—namely, the regression of case histories designated as liquefaction or no liquefaction based on the observation or lack thereof of surficial liquefaction manifestations.

In implementing the procedure, the normalized cyclic stress ratio (CSR^*), or seismic demand, and the normalized cyclic resistance ratio (CRR^*), or soil capacity, are used to compute a factor of safety against liquefaction (FS_{liq}) at a given depth in a soil profile:

$$FS_{liq} = \frac{CRR^*}{CSR^*} \tag{1}$$

where CSR^* = cyclic stress ratio normalized to the duration of an M_w7.5 event and corrected to an effective overburden stress of 1 atm and level-ground conditions; and CRR^* = cyclic resistance ratio derived using field case histories normalized to the same conditions as CSR^* and correlated to normalized in-situ test metrics (e.g., Whitman 1971; Seed and Idriss 1971; Robertson and Wride 1998; Cetin et al. 2004, 2018; Moss et al. 2006; Idriss and Boulanger 2008; Kayen et al. 2013; Boulanger and Idriss 2012, 2014; Green et al. 2019; among many others). These in-situ test metrics include normalized standard penetration test (SPT) blow count (N_{160cs}), normalized cone penetration test (CPT) tip resistance

[1]Graduate Student, Dept. of Civil and Environmental Engineering, Virginia Tech, Blacksburg, VA 24061. Email: usneha@vt.edu

[2]Professor, Dept. of Civil and Environmental Engineering, Virginia Tech, Blacksburg, VA 24061 (corresponding author). ORCID: https://orcid.org/0000-0002-5648-2331. Email: rugreen@vt.edu

[3]Professor, Dept. of Civil and Environmental Engineering, Virginia Tech, Blacksburg, VA 24061. ORCID: https://orcid.org/0000-0002-8384-4721. Email: adrianrm@vt.edu

[4]Assistant Professor, Dept. of Civil and Environmental Engineering, Univ. of Washington, Seattle, WA 98195. Email: bwmaurer@uw.edu

Note. This manuscript was submitted on June 22, 2022; approved on October 25, 2022; published online on January 12, 2023. Discussion period open until June 12, 2023; separate discussions must be submitted for individual papers. This paper is part of the ***Journal of Geotechnical and Geoenvironmental Engineering***, © ASCE, ISSN 1090-0241.

(q_{c1Ncs}), normalized small-strain shear-wave velocity (V_{S1}), among others.

While models developed using this procedure predict the FS_{liq} at a specific depth in the profile, they do not predict the potential for damage to near-surface infrastructure due to liquefaction, which is a function of the depth and thickness of the liquefied layer(s), as well as FS_{liq} and other factors. Other models have thus separately been proposed to relate liquefaction triggering to damage potential via the prediction of the occurrence/severity of surficial liquefaction manifestation, often in the form of a numerical index, referred to herein as manifestation severity index (MSI) models. One of the earliest such models is the liquefaction potential index (LPI) proposed by Iwasaki et al. (1978), which has been widely used in liquefaction hazard assessments around the world (e.g., Sönmez 2003; Papathanassiou et al. 2005, 2015; Papathanassiou 2008; Baise et al. 2006; Cramer et al. 2008; Hayati and Andrus 2008; Holzer et al. 2006, 2009; Holzer 2008; Yalcin et al. 2008; Chung and Rogers 2017; Dixit et al. 2012; Sana and Nath 2016; among many others). However, retrospective evaluations of LPI for some recent earthquakes (e.g., CE in New Zealand) have shown that it performs inconsistently (Maurer et al. 2014, 2015c, a, d). While there may be several factors leading to this inconsistent performance, such findings nonetheless suggest that LPI has inherent limitations. Some of these limitations include: (1) LPI does not fully account for the contractive/dilative tendency of the soil at moderate to large strains on the potential consequences of liquefaction, illustrated by the fact that the resulting consequences for loose and dense sand deposits having the same depths, thicknesses, and FS_{liq} (for example, $FS_{liq} = 0.8$) would likely be very different, but would have the same LPI value; (2) LPI assumes that a soil stratum does not contribute to surface manifestations unless $FS_{liq} \leq 1$, ignoring that surficial liquefaction manifestations can occur due to elevated excess pore pressures during shaking even when $FS_{liq} > 1$ in a stratum; and (3) LPI does not explicitly account for the influence of non-liquefiable crusts and/or the effects that interbedded nonliquefiable soil strata with high fines content (FC) and/or plasticity have on the severity of surface manifestations. In efforts to address some of the shortcomings of LPI, alternative MSI models have been proposed, such as the Ishihara-LPI (LPI_{ish}) by Maurer et al. (2015d), the liquefaction severity number (LSN) by van Ballegooy et al. (2012, 2014b), and more recently, the Ishihara-LSN (LSN_{ish}) by Upadhyaya et al. (2022a).

LPI_{ish} improves on LPI in that: (1) it explicitly accounts for the influence of a nonliquefiable crust on the severity of surficial manifestation using the Ishihara (1985) H_1–H_2 relationships, which relate the thickness of the non-liquefied capping layer (H_1) requisite to prevent surface manifestation given an underlying liquefied layer having thickness (H_2); and (2) weighs more the contribution of shallower layers in predicting the severity of free-field surface manifestations using a power law depth weighting function (i.e., $1/z$, where z is the depth below the ground surface), as opposed to the linear depth weighting function inherent to the LPI model. As with LPI_{ish}, LSN also uses a power law depth weighting function and conceptually improves on LPI in that: (1) it explicitly accounts for the influence of contractive/dilative tendency of the soil at moderate to large strains on the severity of surface manifestation via the Ishihara and Yoshimine (1992) $\varepsilon_v - D_r - FS_{liq}$ relationship, such that for a given FS_{liq}, as relative density (D_r) increases, postliquefaction volumetric strain (ε_v) decreases; and (2) it considers the contribution of strata with FS_{liq} up to 2 in computing the severity of liquefaction manifestations. The more recently proposed LSN_{ish} model is a merger of the LPI_{ish} and LSN models, in that LSN_{ish} explicitly accounts for the effects of the nonliquefiable crust as well as the influence of the contractive/dilative tendency of the soil at moderate to large strains on the severity of surficial liquefaction via the Ishihara and Yoshimine (1992) $\varepsilon_v - D_r - FS_{liq}$ relationship.

Upadhyaya et al. (2022a) compared the predictive efficacies of the four MSI models discussed (i.e., LPI, LPI_{ish}, LSN, and LSN_{ish}) using the CE liquefaction case-history dataset and found that the models that explicitly account for the influence of contractive/dilative tendency of the soil on the severity of liquefaction surface manifestation (i.e., LSN and LSN_{ish}) did not perform as well as the models that do not account for this tendency (i.e., LPI and LPI_{ish}). As discussed in Upadhyaya et al. (2022a), this may be due to the influence of postliquefaction ε_v potential on the severity of surface manifestation being double counted by LSN and LSN_{ish} models. As discussed in more detail subsequently, double counting is an artifact of the way CRR^* curves are derived and used in conjunction with the MSI models.

The findings by Upadhyaya et al. (2022a) highlight the fact that the existing approach to developing triggering curves is inconsistent with how the curves are used to predict the occurrence and severity of surficial manifestation. The inconsistency arises, at least in part, because the triggering curves are developed from field case histories where the inference of whether or not liquefaction triggered at a depth in the profile is primarily based on the presence or absence of surficial evidence, as mentioned previously. Dobry (1989) hypothesized that this approach to classifying case histories as liquefaction or no liquefaction is reflected in the shape of the CRR^* curve (i.e., the dilative tendencies at moderate to large strains of dense soils inhibit surface manifestations, as opposed to medium dense to dense soils not being susceptible to liquefaction triggering, which is a small to moderate strain phenomenon); the authors concur with this hypothesis. In other words, the fact that liquefaction in denser soils is less likely to manifest at the ground surface is inherently tied to observations made at the ground surface, and thus, is potentially also inherent to the shape and positions of existing triggering curves. If so, the subsequent use of the triggering curves with MSI models to account for factors that influence manifestation, but which are already inherent in the curves, would lead to the double counting of influential factors.

Most fundamentally, the issue with the existing approach to developing liquefaction-triggering curves lies in the interpretation of case histories used to develop the CRR^* curves, which involves considerable subjectivity. The observed surficial manifestations are traditionally linked to a single critical layer within the profile rather than to the entire profile response (i.e., system response; e.g., Cubrinovski et al. 2019). In doing this (i.e., inferring response in a critical layer), an analyst is implicitly using a manifestation model (i.e., a model that describes the relationship between liquefaction at depth and its surficial expression), albeit that manifestation model is not a defined expression, but rather, is a personal judgment. Selection of a critical layer must be made such that its density, depth, thickness, FC, plasticity, and strain potential is consistent with the surficial observation (e.g., Green and Olson 2015). This selection must also be made considering the properties of all other soils in the profile, given their potential to augment or suppress surficial evidence. If this is not accomplished, then embedded in the derived triggering curves will be factors that govern not only triggering but also surface manifestation.

Invariably, different judgments and assumptions are involved in the selection of critical layers and their representative properties, influencing the shape and position of the triggering curve and the associated uncertainty (e.g., Green et al. 2014; Green and Olson 2015). And, because this judgment likely differs among interpreted case histories, is often unstated, and most importantly is not defined by a stated model, it cannot be known what assumptions, factors,

and biases are inherent to the triggering curves. In turn, it is difficult to use the curves to predict the occurrence/severity of surface manifestation in a manner consistent with how the curves were developed. Given the inverse problem presented by surficial evidence, which results from two related but distinct phenomena (i.e., triggering and manifestation), it is highly desirable to develop models for predicting these phenomena within a consistent framework.

Toward that end, this study proposes such a framework for developing a *true* triggering curve (i.e., a triggering curve that is absent of factors influencing surface manifestation severity, to the extent possible). The approach is illustrated by assuming a simple triggering-curve functional form and utilizing a large liquefaction case-history database from the CE in New Zealand comprising predominantly clean to silty sand profiles. The model is derived in conjunction with the LSN_{ish} MSI model such that the factors that influence triggering are separated from the factors that influence the occurrence/severity of surficial manifestations. In deriving the true triggering model in this manner, there is no need to select a single critical layer because the response of the entire soil profile is considered, removing the subjectivity associated with the selection of critical layers and their representative properties. Furthermore, both deterministic and probabilistic variants of the true triggering curves are developed, where the latter quantifies the uncertainties in the field observations and in the parameters that control liquefaction triggering and surficial liquefaction manifestation.

In the following, a summary of the CE liquefaction case history database is presented, followed by a detailed description of the approaches used in deriving the deterministic and probabilistic variants of the true triggering model. Following their derivation, a set of 50 worldwide case histories comprising predominantly clean sand to silty, free-field sand profiles are used to evaluate and validate the efficacy of the proposed framework (i.e., LSN_{ish} in conjunction with the true triggering model).

Canterbury Earthquakes Liquefaction Case-History Database

This study utilizes the large CPT-based liquefaction case-history database from the M_w7.1 September 2010 Darfield earthquake, M_w6.2 February 2011 Christchurch earthquake, and M_w5.7 February 2016 Valentine's Day earthquake, collectively referred to herein as the Canterbury earthquakes (CE), as mentioned previously. From this database, which was largely assembled by Maurer et al. (2014, 2015c, a, b, 2017a, b, 2019; Geyin et al. 2021), about 10,000 relatively well-documented case histories from sites where the severity of liquefaction was well documented after one or more of the aforementioned earthquakes. A detailed description of the quality control criteria used in compiling the case histories is provided by Maurer et al. (2014, 2015c) and Geyin et al. (2021). The severity of surficial liquefaction manifestation at each of these CPT sites was obtained via postearthquake ground reconnaissance and using high-resolution satellite imagery and categorized into one of six different classes following Green et al. (2014): no manifestation, marginal manifestation, moderate manifestation, severe manifestation, lateral spreading, and severe lateral spreading. All CPT soundings and imagery were extracted from the New Zealand Geotechnical Database (NZGD 2016).

The marginal, moderate, and severe categories of manifestation refer to the extent to which the ground surface is covered by liquefaction ejecta (e.g., Green et al. 2014; Maurer et al. 2014, 2015c), as detailed in Table 1. Since the severity of lateral spreading is a function of topography, among other factors, which is not accounted for by any of the MSI models discussed previously, case histories having lateral spreading and severe lateral spreading as the predominant form of manifestation are excluded from this study. Similarly, since the effect of nonliquefiable soils that have high FC and/or plasticity on the severity of surficial liquefaction manifestation is a complex phenomenon that is not accounted for by any of the MSI models discussed previously, to include LSN_{ish}, only case histories having predominantly clean sand to silty sand profiles are considered. Maurer et al. (2015c) found that sites in Christchurch with an average CPT soil-behavior-type index (I_c) for the upper 10 m of the soil profile (I_{c10}) less than 2.05 generally correspond to sites having predominantly clean sands to silty sands. Accordingly, only CPT soundings that have $I_{c10} < 2.05$ were considered in this study. With these considerations, 7,167 CE case histories are used in the analyses presented herein, the locations of which are shown in Fig. 1. Of these, 2,574 cases are from the 2010 M_w7.1 Darfield earthquake, 2,582 cases are from the 2011 M_w6.2 Christchurch earthquake, and 2011 cases are from the 2016 M_w5.7 Valentine's Day earthquake. Furthermore, 38% of the case histories were categorized as no manifestation, and the remaining 62% were categorized as either marginal, moderate, or severe manifestations.

Table 1. Liquefaction severity classification criteria

Classification	Criteria
No liquefaction	No surficial liquefaction manifestation or lateral spread cracking
Minor liquefaction	Small, isolated liquefaction features; streets had traces of ejecta or wet patches less than a vehicle width; <5% of the ground surface was covered by ejecta
Moderate liquefaction	Groups of liquefaction features; streets had ejecta patches greater than a vehicle width but were still passable; 5%–40% of the ground surface was covered by ejecta
Severe liquefaction	Large masses of adjoining liquefaction features, streets impassible due to liquefaction, >40% of the ground surface was covered by ejecta

Source: Data from Green et al. (2014).

Estimation of Peak Ground Acceleration

Peak ground accelerations ($PGAs$) are required to estimate the seismic demand at case history sites. In prior CE studies (e.g., Green et al. 2011, 2014; Maurer et al. 2014, 2015c, a, b, d, 2017a, b, 2019; van Ballegooy et al. 2015; among others), $PGAs$ were obtained using the Bradley (2014) procedure, which combines the unconditional PGA distributions as estimated by the Bradley (2013) ground motion model, the recorded $PGAs$ at the strong motion stations (SMSs), and the spatial correlation of intraevent residuals to compute the conditional $PGAs$ at the sites of interest. However, some of the SMS sites experienced severe liquefaction, especially during the M_w6.2 February 2011 Christchurch earthquake, and the recorded $PGAs$ at these sites are inferred to be associated with high-frequency dilation spikes after liquefaction was triggered. Such $PGAs$ are often higher than the $PGAs$ of the preliquefaction portion of the ground motions and likely higher than the $PGAs$ that would have been experienced at the sites if liquefaction had not been triggered. Since the estimation of PGA is central to liquefaction triggering evaluations, such artificially high $PGAs$ at the liquefied SMSs can result in overestimated $PGAs$ at the nearby case-history sites (hence, overly conservative estimated seismic demands), which in turn can lead to overpredictions of

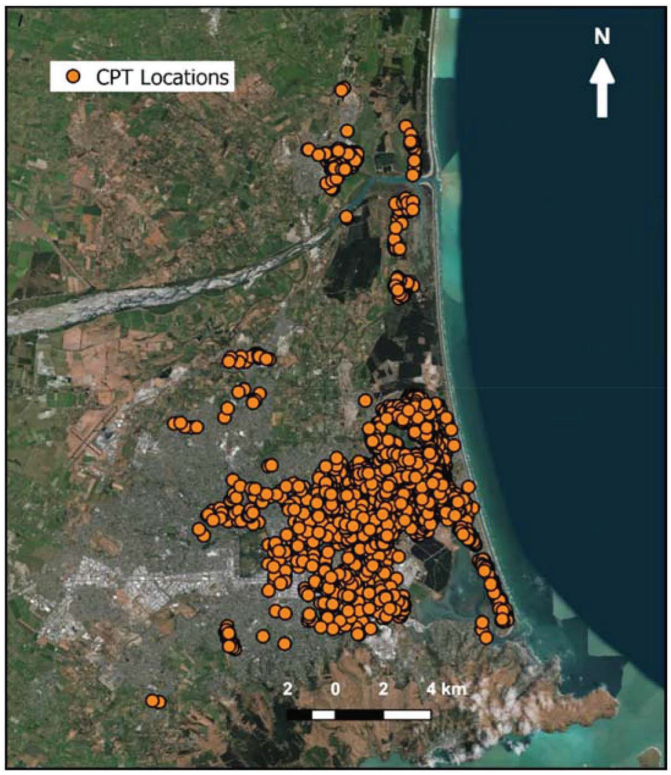

Fig. 1. Map of spatial distributions of CPT sounding locations from CE. (Microsoft Bing screenshot reprinted with permission from Microsoft Corporation, base image data © 2021 Microsoft Corporation, Earthstar Geographics SIO.)

the severity of surficial liquefaction manifestations. Wotherspoon et al. (2014, 2015) identified four such SMSs (i.e., CBGS, CCCC, NNBS, and REHS) where the recorded *PGAs* were higher than the preliquefaction *PGAs* for the 2011 Christchurch earthquake and suggested revised *PGAs* for those stations. Upadhyaya et al. (2019b) investigated the influence of using these revised *PGAs* at the liquefied SMSs on the predicted severity of surficial liquefaction at select case history sites and found that a significant number of case histories were being overpredicted due to overestimated *PGAs*. Accordingly, this study uses the revised preliquefaction *PGAs* at the liquefied SMSs to estimate *PGAs* at the CPT locations.

Estimation of Ground-Water Table Depth

Accurate estimation of the ground-water table (GWT) depth is critical to any liquefaction hazard assessment. GWT depths were estimated at each case-history site at the time of each earthquake using GWT water models that were developed from a large regional network of monitoring wells and river gauges (e.g., van Ballegooy et al. 2014a). These GWT depths, which are available for each of the three earthquakes from NZGD (2016), were used to infer the depth of saturation for assessing liquefaction susceptibility and for computing CSR^*. While the methods used to estimate *PGAs* and GWT depths are arguably rigorous in the context of past precedent, it should be emphasized that these estimates are median values and that measurement uncertainties are not explicitly modeled. For a more extensive discussion of CE *PGA* and GWT estimates, the reader is referred to Geyin et al. (2021).

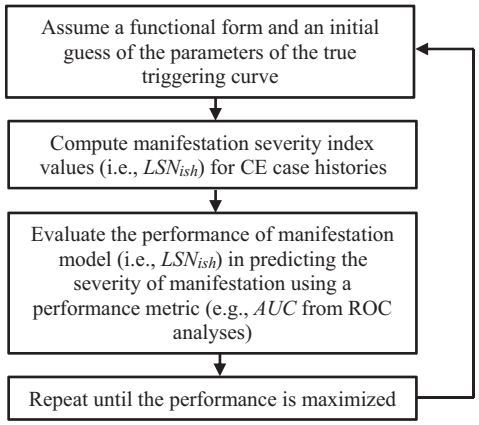

Fig. 2. Flowchart showing the approach for deriving a true liquefaction triggering curve within the LSN_{ish} model.

Derivation of True Liquefaction Triggering Model in Conjunction with the LSN_{ish} Model

Deterministic Approach

Utilizing 7,167 CE liquefaction case histories, a true triggering model is determined using an iterative approach in conjunction with the LSN_{ish} model such that its predictive efficiency is maximized. The approach used in deriving the true triggering model is summarized in Fig. 2 and discussed in detail in the following.

Functional Form of the True Triggering Curve

As discussed in the *Introduction*, the shapes of traditionally derived triggering curves are likely influenced by the dilative tendencies at moderate to large strains of medium dense to dense soils that inhibit surficial liquefaction manifestations when liquefaction is triggered (e.g., Dobry 1989). As a result, alternative functional forms for a true triggering curve are considered in this study (i.e., true triggering curve—a triggering curve whose shape is not influenced by surficial manifestation). However, despite the robustness of the case history database, some judgment is required in selecting the functional form of the true triggering curve. Based on the reinterpretation of a detailed field case history by Dobry (1989) and the laboratory test data from a detailed study by Ulmer (2019) and Ulmer et al. (2022), the authors deemed it reasonable to assume as a first approximation that the true triggering curve plots as a straight line. Note, however, that the proposed framework for deriving the true triggering curve is not limited to any given functional form. But, the functional form of the true triggering curve should be guided by fundamental liquefaction mechanics (e.g., Dobry 1989; Ulmer 2019; Ulmer et al. 2022).

Dobry (1989) reinterpreted the Herber Road Site case history originally presented by Youd and Bennett (1983). The site was subjected to intense shaking during 1979, M_w6.6 Imperial Valley, California, earthquake, with a portion of the site exhibiting surficial liquefaction manifestations and another portion not. However, detailed numerical effective stress site-response analyses predicted high excess pore water pressures across the entire site. Dobry (1989) hypothesized that it was the dilative tendency at moderate to large strains of dense soils underlying a portion of the site that inhibited surficial liquefaction manifestations at portions of the site, despite these denser soils having liquefied.

Ulmer et al. (2022) performed stress-controlled, constant-volume cyclic direct simple shear tests on air-pluviated Monterey No. 0/30 sand having D_r ranging from 25% to 80% and an initial

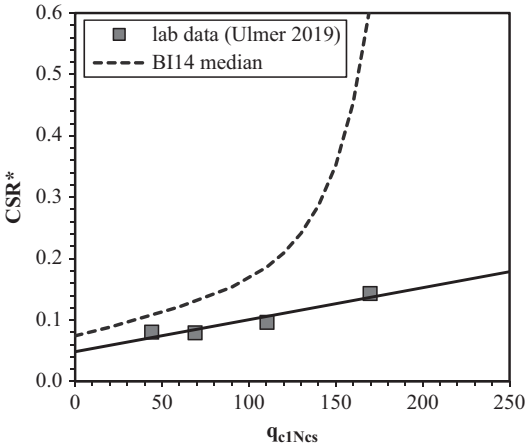

Fig. 3. CSR^* versus q_{c1Ncs} data from laboratory tests of Ulmer (2019) and Ulmer et al. (2022) along with the best fit CRR^* curve (solid black line) as well as the BI14 median CRR^* curve.

vertical effective confining stress (σ'_{vo}) equal to 100 kPa. Liquefaction triggering was defined as residual excess pore water pressure ratio (r_u) equal to 0.98. The CSR^* corresponding to the number of cycles to liquefaction (N_L) for an M_w7.5 event (i.e., $N_L = 14$; Green et al. 2019) were obtained from test data grouped according to their D_r. Estimating the equivalent q_{c1Ncs} values using the $q_{c1ncs} - D_r$ correlation by Idriss and Boulanger (2008), the laboratory test-based triggering curve is plotted in Fig. 3. As may be observed in this figure, the laboratory data imply that the triggering curve can be reasonably approximated as a straight line, and this is especially true when an r_u – based criterion is used to interpret the laboratory data (e.g., $r_u = 0.98$). For comparison purposes, the Boulanger and Idriss (2014) [BI14] median CRR^* curve is also plotted in Fig. 3.

Thus, as a first and reasonable approximation, the functional form of the true CRR^* curve is defined as

$$CRR^* = \frac{q_{c1Ncs}}{a_1} + a_2 \tag{2}$$

where a_1 and a_2 = parameters that define the slope (where: slope $= 1/a_1$) and the y-intercept of the true triggering curve, respectively, and are derived within an optimization algorithm such that the predictive efficacy of LSN_{ish} is maximized for the CE dataset used in this study. We emphasize that the choice of a linear functional form for the true CRR^* curve is an assumption made by the authors, properly justified by the laboratory test data cited in the previous paragraph. However, the framework proposed herein would be equally applicable should other choices be made for the functional form of the true CRR^* curve. The predictive efficacy of LSN_{ish} is assessed using receiver operating characteristic (ROC) analyses, an overview of which is presented in the following section. LSN_{ish} can be computed as

$$LSN_{ish} = \int_{H_1}^{z_{max}} [F(\varepsilon_v) \cdot w(z)] dz \tag{3a}$$

where H_1 = thickness of the nonliquefiable crust in m (Ishihara 1985); z = depth below the ground surface in m; z_{max} = maximum depth (also in m) of the liquefied soil that is assumed to contribute to surficial manifestations (i.e., 20 m); and ε_v = volumetric strain in percent; and

$$w(z) = \frac{36.929}{z} \tag{3b}$$

$$F(\varepsilon_v) = \begin{cases} \dfrac{\varepsilon_v}{5.5} & if\ FS_{liq} \le 2 \quad and \quad H_1 \cdot m(\varepsilon_v) \le 3 \\ 0 & otherwise \end{cases} \tag{3c}$$

$$m(\varepsilon_v) = \exp\left(\frac{0.7447}{\varepsilon_v}\right) - 1; \qquad m(\varepsilon_v < 0.16) = 100 \tag{3d}$$

$F(\varepsilon_v)$ and $w(z)$ = functions weighting the respective contributions of ε_v and z on the severity of surficial liquefaction manifestation; ε_v is estimated as a function of FS_{liq} and q_{c1Ncs} using the Zhang et al. (2002) procedure, which is based on the Ishihara and Yoshimine (1992) $\varepsilon_v - D_r - FS$ data; FS_{liq} is computed using Eq. (1) wherein CSR^* is computed following the Green et al. (2019) procedure in conjunction with the modified overburden correction factor (K_γ) formulation recently proposed by Green et al. (2022). Inherent to this process, soils having a CPT soil behavior type index (I_c) exceeding 2.5 are considered nonliquefiable (e.g., Maurer et al. 2017b, 2019). Note that this is a Christchurch-specific criterion proposed by Maurer et al. (2019), which slightly differs from the commonly used $I_c > 2.6$ (e.g., Robertson and Wride 1998). Moreover, FC was estimated using the Christchurch-specific $I_c - FC$ correlation proposed by Maurer et al. (2019).

Overview of ROC Analyses

Receiver operating characteristics (ROC) analyses have been widely used to evaluate the performance of diagnostic models, including extensive use in medical diagnostics (e.g., Zou 2007) and to a much lesser degree in geotechnical engineering (e.g., Oommen et al. 2010; Maurer et al. 2015c, a, b, 2017a, b, 2019; Green et al. 2017; Zhu et al. 2017; Upadhyaya et al. 2018, 2019a, 2021, 2022a, b). In cases where the distribution of positives (e.g., cases of observed surficial liquefaction manifestation) and negatives (e.g., cases of no observed surficial liquefaction manifestations) overlap [e.g., Fig. 4(a)], ROC analyses can be used to: (1) identify the optimum diagnostic threshold (e.g., LSN_{ish} value corresponding to a specified liquefaction manifestation severity threshold); and (2) assess the relative efficacy of competing diagnostic models, independent of the thresholds used. A ROC curve is a plot of the true positive rate (R_{TP}) (i.e., surficial liquefaction manifestation was observed, as predicted) versus the false positive rate (R_{FP}) (i.e., surficial liquefaction manifestation is predicted, but was not observed) for varying MSI threshold values (e.g., LSN_{ish}). A conceptual illustration of ROC analysis, including the relationship among the distributions for positives and negatives, the MSI threshold value, and the ROC curve, is shown in Fig. 4.

In ROC curve space, a diagnostic test that has no predictive ability (i.e., a random guess) results in an ROC curve that plots as a 1:1 line through the origin. In contrast, a diagnostic test that has a perfect predictive ability (i.e., a perfect model) plots along the left vertical and upper horizontal axes, connecting at the point (0,1) and indicates the existence of a threshold value that perfectly segregates the dataset (e.g., all cases with observed surficial manifestation will have LSN_{ish} above the threshold and all cases with no observed surficial manifestation will have LSN_{ish} below the threshold). The area under the ROC curve (AUC) can be used as a metric to evaluate the predictive performance of a diagnostic model (e.g., LSN_{ish}), whereby a higher AUC indicates better predictive capabilities (e.g., Fawcett 2006). As such, a random guess returns an AUC of 0.5, whereas a perfect model returns an AUC of 1. The optimum operating point (OOP) in a ROC analysis is defined as the threshold value (e.g., threshold LSN_{ish}) that minimizes the rate of

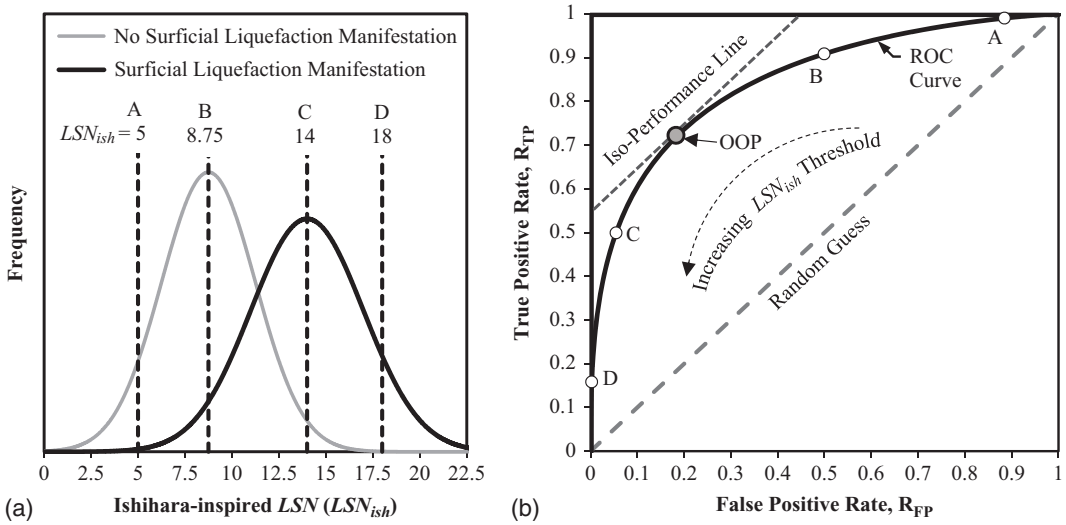

Fig. 4. Conceptual illustration of ROC analyses: (a) frequency distributions of surficial liquefaction manifestation and no surficial liquefaction manifestation observations as a function of LSN_{ish}; and (b) corresponding ROC curve. (Reprinted from *Soil Dynamics and Earthquake Engineering*, Vol. 76, B. W. Maurer, R. A. Green, M. Cubrinovski, and B. A. Bradley, "Fines-content effects on liquefaction hazard evaluation for infrastructure in Christchurch, New Zealand," pp. 58–68, © 2015, with permission from Elsevier.)

misprediction [i.e., $R_{FP} + (1 - R_{TP})$]. Contours of the quantity $[R_{FP} + (1 - R_{TP})]$ are isoperformance lines joining points of equivalent performance in ROC space, as illustrated in Fig. 4(b).

Initially, ROC analyses were performed iteratively within an optimization function to obtain regression parameters a_1 and a_2 that maximized the AUC for the CE dataset. However, even for the assumed straight-line functional form of the true triggering curve, the case history data does not fully constrain both parameters at the same time. Thus, the slope of the true triggering curve is assumed equal to the slope of the laboratory-based CRR^* curve (i.e., $a_1 = 1919.2$) and the only parameter that is regressed using the case history data is the y-intercept, which is found to be equal to 0.09 (i.e., $a_2 = 0.09$). The authors realize that setting any constraints on the shape of the true triggering curve entails considerable judgment, but the assumed simplistic functional form and slope of the true triggering curve are deemed reasonable first approximations and also serve the purpose of illustrating the proposed framework for deriving true triggering curves. Note, however, that the proposed framework for deriving the true triggering curve is not limited to these constraints. Fig. 5 shows the true triggering curve derived in conjunction with the LSN_{ish} model. The resulting true triggering model separates cases of surficial and no surficial liquefaction manifestation (i.e., yes and no cases) and is therefore analogous to the median CRR^* curve. For comparison purposes, the BI14 median CRR^* curve is also shown in Fig. 5. It can be seen that the y-intercept of the true triggering curve is very similar to that of the BI14 median CRR^* curve. This gives credence to the proposed approach because separating factors that control surficial liquefaction manifestation would intuitively result in a triggering curve that lies close to the traditionally develop CRR^* curves at q_{c1Ncs} values corresponding to loose soils but below traditionally developed CRR^* curves at q_{c1Ncs} values corresponding to medium dense to dense soils.

Threshold values of manifestation severity indices are commonly used to perform deterministic assessments of liquefaction damage potential at sites. However, these threshold values are specific to the triggering and MSI models used (e.g., Maurer et al. 2015a; Upadhyaya et al. 2022b). Accordingly, ROC analyses were performed on the CE dataset to compute optimum threshold values for LSN_{ish} (in conjunction with the true triggering curve derived herein) considering: (1) only the occurrence of surficial manifestation (i.e., yes or no); and (2) different severities of surficial liquefaction manifestation (i.e., minor, moderate, or severe). These optimum threshold LSN_{ish} values are summarized in Table 2. It should be noted that these threshold values are determined using

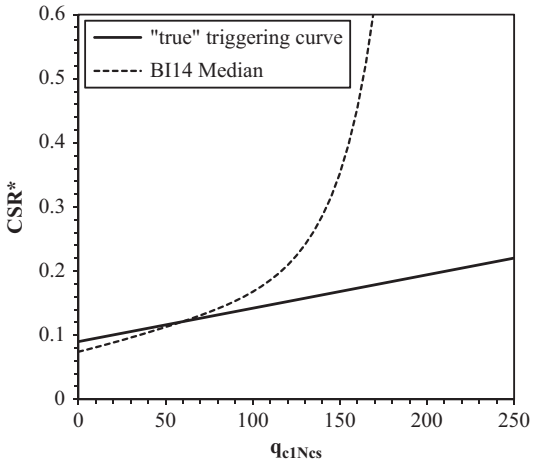

Fig. 5. True triggering curve derived within the LSN_{ish} model plotted along with the BI14 median CRR^* curve.

Table 2. Optimum LSN_{ish} thresholds for different severities of surficial liquefaction manifestation

Manifestation severity category	Threshold, LSN_{ish}
Any manifestation	4.2
Marginal manifestation	3.1
Moderate manifestation	10.1
Severe manifestation	23.0

free-field site case histories having predominantly clean sand to silty sand profiles and are not recommended for use at sites having predominantly silty and clayey soil mixtures (i.e., soils with high FC and/or high plasticity) or developed sites with deep foundations, for example.

Probabilistic Approach

The deterministic approach presented in the previous section is expanded into a probabilistic framework, such that the true triggering model reflects the uncertainties in field observations and in the parameters that control liquefaction triggering and surface manifestation. Probabilistic triggering relationships for SPT-, CPT-, and V_S-based in-situ testing methods have been proposed by a number of researchers (e.g., Juang et al. 2002; Cetin et al. 2002, 2004, 2018; Moss et al. 2006; Idriss and Boulanger 2010; Boulanger and Idriss 2012, 2014; among others). The limit state function, which represents the boundary between liquefaction and no liquefaction regions in the space of predictor variables, is generally expressed as (Cetin et al. 2002, 2004):

$$g(X;\Theta,\varepsilon) = \hat{g}(X;\Theta) + \varepsilon \tag{4}$$

where $\hat{g}(\cdot)$ = approximation to the true limit state function g; X = vector of predictor variables that quantify the soil capacity (e.g., where q_{c1Ncs} is used as an index for soil capacity) and the seismic demand (e.g., CSR^*); Θ = parameters of the limit state function; and ε = error term which is traditionally assumed to be normally distributed with a mean of zero and a standard deviation σ_ε.

By definition, $g(X;\Theta,\varepsilon)$ takes zero or negative values when liquefaction is predicted to trigger and positive values when liquefaction is not predicted to trigger. Assuming that the predictive variables and the parameters of the limit state function are known, the probability of liquefaction triggering (P_L) can be expressed as (Cetin et al. 2002)

$$P_L = \left(-\frac{\hat{g}(X;\Theta)}{\sigma_\varepsilon}\right) \tag{5}$$

where $\Phi(\cdot)$ = standard normal cumulative distribution function.

In past studies, the parameter set Θ has been determined using liquefaction and no liquefaction case histories. However, as discussed previously, this designation of liquefaction and no liquefaction is based almost exclusively on observations of surficial liquefaction manifestations, not on whether liquefaction was triggered at a depth in the soil profile. In this study, the parameters of the liquefaction triggering relationship are determined using a probabilistic framework that includes a surface manifestation model, therefore allowing for the development of a true liquefaction triggering model. The proposed approach is detailed in the following section.

Limit State Function for Liquefaction Triggering

The following form of the limit-state function for liquefaction triggering is used:

$$g(q_{c1Ncs}, CSR^*;\Theta,\varepsilon) = \ln(CRR^*) - \ln(CSR^*) + \varepsilon \tag{6}$$

As mentioned previously, the CRR^* curve derived using the deterministic approach is analogous to a median CRR^* curve. To maintain consistency between the shape and position of the CRR^* curve from the deterministic and probabilistic approaches, the probabilistic relationship for CRR^* is expressed as

$$CRR^* = \exp\left[\ln\left(\frac{q_{c1Ncs}}{a_1} + a_2\right) + \sigma_\varepsilon \cdot \Phi^{-1}(P_L)\right] \tag{7}$$

where $a_1 = 1{,}919.2$ and $a_2 = 0.09$; σ_ε is treated as an unknown model parameter that is estimated using regression analyses; $\Phi^{-1}(\cdot)$ = inverse of the standard cumulative normal distribution; and P_L = probability of liquefaction triggering. Note that the implicit assumption is that the median true liquefaction curve is given by the deterministic curve obtained previously, and only the uncertainty around the median curve (σ_ε) is obtained from the probabilistic analysis. This choice is justified subsequently in discussing the regression approach.

Probabilistic Definition of Surficial Liquefaction Manifestation

For a given soil profile, the probability of surficial liquefaction manifestation, $P(S)$, is defined as

$$P(S) = \int P(S|LSN_{ish}) \cdot f_{LSN_{ish}}(l|\Theta;X) \cdot dl \tag{8}$$

where S = binary random variable that denotes surficial liquefaction manifestation; $P(S|LSN_{ish})$ = conditional probability of surficial liquefaction manifestation given an LSN_{ish} value and is akin to defining LSN_{ish} thresholds in the deterministic approach; and $f_{LSNish}(l|\Theta;X)$ = probability density function (PDF) of LSN_{ish} that is computed using the probabilistic model in Eq. (7).

The conditional probability of surficial liquefaction manifestation, $P(S|LSN_{ish})$, is defined using a logistic regression type model (e.g., Papathanassiou 2008; Juang et al. 2010; Chung and Rogers 2017) given by:

$$P(S|LSN_{ish}) = \frac{1}{1 + e^{-(B_0 + B_1 \cdot LSN_{ish})}} \tag{9}$$

where B_0 and B_1 = model parameters that are determined using regression. Thus, in addition to σ_ε, B_o and B_1 are two more parameters that are obtained through regression.

The PDF of LSN_{ish} (i.e., f_{LSNish}) is obtained by mapping the uncertainties in the liquefaction triggering relationship (i.e., σ_ε) to the uncertainties in the LSN_{ish} model. In this process, random samples of ε are generated from a normal distribution with mean zero and standard deviation σ_ε [Eq. (6)]. However, instead of using blind sampling, which is computationally expensive, a reduced sampling approach is adopted. In this approach, probabilities between 0 and 1 are divided into N number of equally spaced bins, and samples of ε are obtained as the inverse of the normal cumulative distribution function (CDF) at the middle of each bin. For each sample (ε_i), the CRR^* value is computed using Eq. (7) and $LSN_{ish,i}$ is computed using Eq. (3). The repeated application of this approach for each of the N bins results in a distribution of LSN_{ish} for each case history. It is assumed that LSN_{ish} generally follows a lognormal distribution. However, since LSN_{ish} can take zero values, f_{LSNish} is defined using a combination of a Dirac delta function at $LSN_{ish} = 0$ [i.e., $\delta(LSN_{ish})$] and a lognormal distribution for $LSN_{ish} > 0$ with parameters $\mu_{\ln(LSNish)}$ and $\sigma_{\ln(LSNish)}$ that define the mean and standard deviation of the natural logarithm of LSN_{ish}, respectively:

$$f_{LSN_{ish}} = P(LSN_{ish} = 0) \cdot \delta(LSN_{ish}) + \omega' \cdot f_{LSN_{ish}|LSN_{ish}>0} \tag{10a}$$

where

$$\omega' = 1 - P(LSN_{ish} = 0) \tag{10b}$$

$$\delta(LSN_{ish}) = \begin{cases} 0 & for\ LSN_{ish} \neq 0 \\ \infty & for\ LSN_{ish} = 0 \end{cases} \quad (10c)$$

$$\int_{-\infty}^{\infty} \delta(LSN_{ish}) dl = 1 \quad (10d)$$

In Eq. (10*a*), $P(LSN_{ish} = 0)$ is the probability of LSN_{ish} being zero and can be obtained as the ratio of the number of samples of ε that result in $LSN_{ish} = 0$ to the total number of samples (N).

To determine the number of probability bins (N) needed to obtain estimates of $P(LSN_{ish} = 0)$, $\mu_{\ln(LSNish)}$, and $\sigma_{\ln(LSNish)}$ that are comparable to those obtained from blind sampling, sensitivity analyses are performed on a few randomly selected case histories from the CE dataset, wherein N is varied between 25 and 1,000. It is found that $N = 100$ resulted in reasonable estimates of the aforementioned parameters.

Regression Approach

The unknown parameters of the liquefaction triggering relationship (i.e., σ_ε) and the $P(S|LSN_{ish})$ model parameters (i.e., B_o and B_1) are estimated simultaneously using maximum likelihood estimation, where the likelihood function is defined as

$$L(\Theta) = \prod_{manifestation} P(S) \times \prod_{no\ manifestation} [1 - P(S)] \quad (11)$$

In performing the regression analyses, it is assumed that the input parameters are exact (i.e., the uncertainties in the input parameters are not incorporated in the regression analyses). The solution obtained by maximizing the likelihood function [i.e., Eq. (11)] indicates that the case history data themselves are not sufficient to simultaneously constrain all the parameters of the triggering relationship (a_1, a_2, σ_ε) and the surface manifestation model parameters (B_0 and B_1). This is also likely due, in part, to the correlation between the regression parameters. For this reason, parameters a_1 and a_2 were obtained from the deterministic approach detailed previously. When an attempt is made to constrain all the remaining parameters simultaneously, the regression results in all the uncertainty assigned to the manifestation model, and the resulting uncertainty in the triggering model is negligible. One way to partition the uncertainty between the triggering and manifestation models is to constrain the $P(S|LSN_{ish})$ curve such that $P(S|LSN_{ish}) \geq 0.99$ for $LSN_{ish} \geq 23$ (Fig. 7). Note that $LSN_{ish} = 23$ is the deterministic threshold for severe liquefaction manifestation and thus it is reasonable to assume that the probability of any surficial liquefaction manifestation is close to 1 if this threshold is exceeded. From the maximum likelihood regression analyses, it is found that $\sigma_\varepsilon = 0.243$, $B_0 = -2.77$, and $B_1 = 0.37$. The resulting true probabilistic liquefaction-triggering relationships are

$$CRR^* = exp\left[\ln\left(\frac{q_{c1Ncs}}{1919.2} + 0.09\right) + 0.243 \cdot \Phi^{-1}(P_L)\right] \quad (12)$$

and

$$P_L = \Phi\left[-\frac{\ln(\frac{q_{c1Ncs}}{1919.2} + 0.09) - \ln(CSR^*)}{0.243}\right] \quad (13)$$

The true triggering curves corresponding to $P_L = 15\%$, 50%, and 85% are shown in Fig. 6, and the regressed $P(S|LSN_{ish})$ curve is shown in Fig. 7. Also shown in Fig. 7 are the observed probabilities of surficial manifestation computed by grouping the LSN_{ish} values into multiple equally spaced bins. These probabilities are computed as the ratio of cases with observed manifestation to the total number of cases in each bin. There is a good agreement

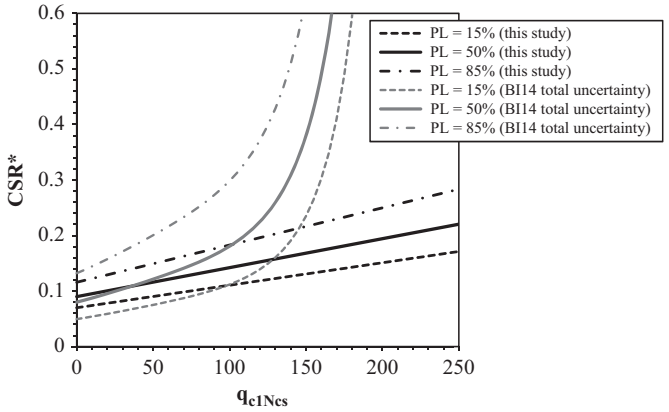

Fig. 6. Probabilistic true liquefaction triggering curves derived in conjunction with the LSN_{ish} model. Also shown are the BI14 total uncertainty CRR^* curves for clean sand ($FC \leq 5\%$), regressed by Green et al. (2016).

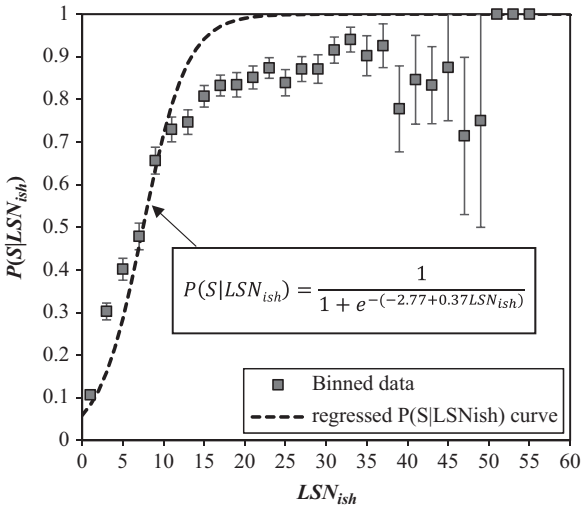

Fig. 7. Probability of surficial liquefaction manifestation as a function of LSN_{ish} along with the observed binned data.

between the regressed $P(S|LSN_{ish})$ curve and the observed binned data for $P(S|LSN_{ish}) < 0.8$. An implication of this observation is that when $P(S|LSN_{ish}) > 0.8$, it is assumed that it is almost certain that surface manifestation occurs, which is a reasonably conservative outcome. Moreover, as mentioned previously, in deriving the probabilistic triggering relationship, it is assumed that the input parameters to the model are exact. As a result, the uncertainty in the triggering curve indirectly reflects total uncertainty (i.e., the uncertainties in both the input parameters and the model uncertainty). Since existing triggering relationships are often presented in terms of model uncertainty alone (e.g., Boulanger and Idriss 2014), a direct comparison of the true triggering curves regressed here and existing probabilistic triggering curves cannot be made. However, Green et al. (2016) used the case history data of BI14 and regressed probabilistic triggering relationships for clean sands (i.e., $FC \leq 5\%$) in terms of total uncertainty, which are also shown in Fig. 6. It can be seen that the uncertainty in the true triggering model regressed herein is smaller than the total uncertainty computed by Green et al. (2016) for the BI14 triggering relationship. This is likely because the $P(S|LSN_{ish})$ model (Fig. 7) accounts

Table 3. Optimum P(S) threshold for different severities of surficial liquefaction manifestation

Manifestation severity category	Threshold, P(S)
Any manifestation	0.4
Marginal manifestation	0.3
Moderate manifestation	0.6
Severe manifestation	0.7

for uncertainties associated with factors influencing the surficial liquefaction manifestation, hence reducing the uncertainty in the triggering relationship. Finally, the use of the $P(S|LSN_{ish})$ relationship shown in Fig. 7 inherently implies that the threshold shear strain is exceeded; when this is not the case, $P(S|LSN_{ish}) = 0$.

Similar to the definition of optimum LSN_{ish} thresholds for determining surface manifestation in the deterministic approach (Table 2), optimum threshold P(S) values are also assessed by performing ROC analyses on the CE dataset, considering: (1) only the occurrence of surficial manifestation (i.e., yes or no); and (2) different severities of surficial liquefaction manifestation (i.e., minor, moderate, or severe). These threshold P(S) values are summarized in Table 3.

Evaluation of Case Histories

CE Liquefaction Case Histories

To compare the efficacies of the true triggering model with that of the BI14 model, the median curves are used in conjunction with the LSN_{ish} formulation to analyze the CE dataset; the associated ROC curves are plotted in Fig. 8. Note that for consistency in implementing the models with how they were derived, CSR^* is computed using Green et al. (2019) when the true triggering curve is used and Boulanger and Idriss (2014) when the BI14 median CRR^* curve is used. It can be seen that the AUC associated with the true triggering curve derived herein is 6.8% higher than the BI14 median CRR^* curve. These findings suggest that for the dataset assessed, the true triggering curve is more efficacious than the BI14 median CRR^* curve in distinguishing sites with and without surficial liquefaction manifestation when used in conjunction with the LSN_{ish} model. Specifically, and given the definition of AUC, the probability of sites with manifestations having a higher LSN_{ish} value than sites without manifestations increased by 6.8%.

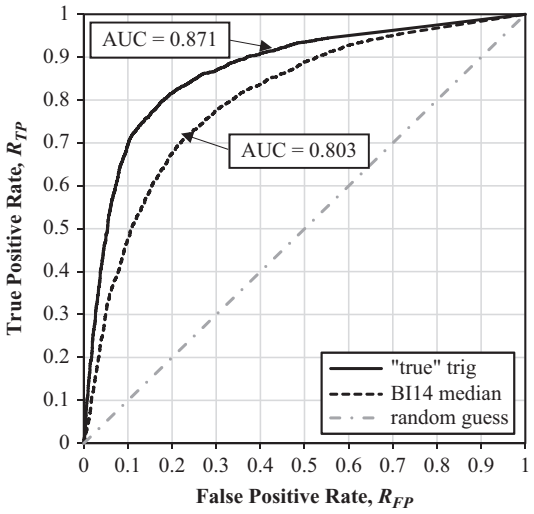

Fig. 8. ROC curves for the true triggering curve and the BI14 CRR^* curve, operating within LSN_{ish}.

Evaluation of 50 Worldwide Liquefaction Case Histories

As detailed previously, the true triggering model presented in this study is developed solely using the CE dataset, which contains case histories resulting from only three earthquakes and from limited geological and seismological environments. Thus, to evaluate the efficacy of the true triggering curve used in conjunction with LSN_{ish} for nonCE settings, 50 worldwide case histories having profiles comprising predominantly clean sand to silty sand (i.e., $I_{c10} < 2.05$) are compiled from the existing literature. A summary of these 50 worldwide case histories is presented in Table S1 in the electronic supplement. These 50 case histories comprise 29 liquefaction and 21 no-liquefaction cases from six different earthquakes from around the world.

For each of these 50 case histories, LSN_{ish} values are computed using both the deterministic true triggering relationship derived herein as well as the BI14 median triggering relationship, where soils having $I_c > 2.6$ are considered nonliquefiable. Using the optimum threshold values of LSN_{ish} for distinguishing cases with and without manifestation evaluated using: (1) the true triggering relationship (e.g., Table 2); and (2) BI14 median triggering relationship (e.g., LSN_{ish} threshold of 3.6 as computed by Upadhyaya et al. 2022a), the overall accuracy (i.e., the ratio of the number of accurately predicted cases to the total number of cases) is computed for each model. Note that the liquefaction manifestation severity for the worldwide case histories is only categorized as either yes or no, and thus, the threshold LSN_{ish} distinguishing any manifestation from no manifestation is used to compute the overall accuracy. It is found that the overall accuracies of LSN_{ish} used in conjunction with the true triggering relationship and the BI14 median triggering relationship are both 66% (i.e., both the true triggering and the BI14 median triggering relationships accurately predicted 33 out of 50 case histories). These findings suggest that for the worldwide dataset, the true triggering relationship is equally efficacious as the BI14 triggering relationship in predicting the occurrence of surficial liquefaction manifestation when operating in conjunction with the LSN_{ish} model. However, as elaborated on in the next section, the ability of the true liquefaction curve to be used in conjunction with MSI models that account for complex free-field soil profile stratigraphies or developed sites is a significant advantage over traditionally developed triggering curves.

Using the probabilistic approach for assessing the severity of surficial liquefaction manifestation (or, liquefaction damage potential) proposed herein, the probability of surficial liquefaction manifestation, $P(S)$, is computed in conjunction with the true triggering relationship for each of the 50 case histories [i.e., Eq. (8)]. Using the optimum threshold $P(S)$ that distinguishes any manifestation from no manifestation determined in the previous section (e.g., Table 3), the overall accuracy of $P(S)$ in predicting the occurrence of surficial liquefaction manifestation for the worldwide case histories is 66%. This is the exact same as that obtained using the deterministic threshold LSN_{ish}, implying that the application of the proposed deterministic and probabilistic approaches is self-consistent. However, the advantage of using the probabilistic approach is that it can be also used in conjunction with seismic-hazard analyses to estimate the annual exceedance frequencies or return periods of liquefaction triggering or manifestation.

Discussion and Conclusions

This paper proposed an internally consistent framework for predicting liquefaction triggering and the resulting severity of surficial manifestation. Specifically, this paper presented a methodology to derive a true liquefaction triggering model consistent with a defined manifestation model (i.e., LSN_{ish}) such that factors influential to triggering and manifestation are handled more rationally and consistently. Moreover, the proposed methodology removes some of the subjectivity associated with interpreting field case histories (e.g., the selection of critical layers and their representative properties). Toward this end, the cumulative response of the entire soil profile is linked to the observed surficial liquefaction manifestation. Utilizing 7,167 CPT liquefaction case histories from three recent earthquakes that impacted the Canterbury region of New Zealand, deterministic and probabilistic variants of the true triggering model were developed in conjunction with the recently proposed LSN_{ish} model.

The case history data were not sufficient to constrain all parameters of the triggering and manifestation relationships. This is largely because the CE dataset used in this study comprises case histories resulting from only three earthquakes from the same geographic region. As a result, the case histories represent limited seismological and geological variability. Thus, it is necessary to use several assumptions to constrain some of the parameters of the triggering and manifestation relationships. Specifically, the functional form of the true triggering curve is assumed to be a straight line. This assumed functional form is deemed reasonable based on a reinterpretation of a detailed field case history by Dobry (1989). Furthermore, Ulmer (2019) and Ulmer et al. (2022) analyzed laboratory test data and showed that when an r_u-based criterion is used to interpret the data (e.g., $r_u = 0.98$), the resulting triggering curve has a linear trend and a relatively flat slope. However, when strain-based criteria are used to interpret the same laboratory test dataset, the resulting triggering curves are more nonlinear at higher D_r values or have steeper slopes if linear trends are fit to the data. The deviation from linearity at high D_r values can arguably be characterized as being related to liquefaction manifestation and not triggering and is appropriately accounted for by the LSN_{ish} MSI model. Regardless, it is emphasized that the proposed framework for deriving the true triggering curve is not limited to any given functional form, but rather, the framework allows the functional form of the true triggering curve to be guided by fundamental liquefaction mechanics, as the authors believe is the case in this study.

It was shown that the prediction efficacy of the true triggering model derived herein is ~7% higher than the BI14 median triggering model for the CE dataset when the models are used in conjunction with the LSN_{ish} MSI model to predict the severity of surficial liquefaction manifestations. For context, this improvement for CE case histories is larger than that observed between any existing triggering models (e.g., Robertson and Wride 1998; Moss et al. 2006; Boulanger and Idriss 2014), as shown by Geyin et al. (2020). In other words, the improvement suggests a departure from the performance variation observed among existing models that were developed using the traditional approach. However, the comparison of the efficacies of the true versus BI14 triggering models is inherently biased in favor of the true triggering model because it was derived only from the CE dataset, while the BI14 model was derived from 255 worldwide case histories, which includes 50 CE case histories. Accordingly, as a further assessment of the efficacy of the true triggering model, 50 global case histories were analyzed using the true and BI14 triggering models in conjunction with the LSN_{ish} MSI model. It was found that the overall accuracies of the true triggering model and the BI14 median triggering curve were exactly the same (i.e., 66%). Note, however, that the BI14 triggering model was developed using these 50 worldwide case histories, while the true triggering model was not. As a result, this comparison is also inherently biased, although this time in favor of the traditionally developed BI14 triggering model.

The case histories used in the comparisons described comprise predominantly clean sand to silty sand, free-field profiles. However, the ability of the true liquefaction curve to be used in conjunction with MSI models that account for complex soil profile stratigraphies or developed sites with deep foundations, for example, is a significant advantage over traditionally developed triggering curves. Specifically, past studies have shown that the occurrence/severity of surficial liquefaction manifestation is influenced by the presence of nonliquefiable, high FC, high plasticity soil strata (e.g., Maurer et al. 2015c; Upadhyaya et al. 2018, 2022a, b); however, such effects are not accounted for by any of the existing MSI models to include the current LSN_{ish} model. Future developed MSI model(s) that account for the influence of nonliquefiable layers interbedded in liquefiable deposits can be used in conjunction with the proposed true triggering model to better predict the system response of such complex soil profiles. Additionally, MSI models can be developed for the influence of liquefaction at depth on deep foundations, where the distinction between liquefaction at depth versus the severity of surficial liquefaction manifestations is critical. Specific to the LSN_{ish} MSI model, it is envisioned that modifications to the depth weighting factor, $w(z)$, could be made to account for the influence of interbedded clay layers on the severity of surficial liquefaction manifestations and the damage potential of liquefaction at depth on deep foundations. In addition, the use of such a modified LSN_{ish} MSI model with the true triggering model represents an internally-consistent framework for predicting liquefaction triggering and damage potential. In this regard, however, it is again emphasized that traditionally developed liquefaction triggering curves were derived using case histories that were categorized as liquefaction or no liquefaction based on surface manifestations or lack thereof. As a result, the use of traditionally developed triggering curves is inherently limited for assessing the consequences of liquefaction triggering for complex soil profiles and developed sites with deep foundations. Finally, the true liquefaction triggering model can be used in isolation from an MSI model to compute FS_{liq} or P_L versus depth, similar to how traditionally developed triggering models are often used. Toward this end, FS_{liq} or P_L can be computed at each depth for which q_{c1Ncs} are measured or for each stratum in the profile using representative values of q_{c1Ncs} for the strata.

Despite areas where potential improvements can be made (e.g., improved function form used to model the true triggering curve and further developments in MSI models), this paper presents an internally consistent framework for predicting liquefaction triggering and the resulting damage potential, thereby conceptually advancing the state-of-the-art in liquefaction risk assessment.

Data Availability Statement

Some or all data, models, or code that support the findings of this paper are available from the corresponding author upon reasonable request. The CE case history data studied herein are available in digital format from Geyin et al. (2021).

Acknowledgments

This research was funded by National Science Foundation (NSF) Grants CMMI-1751216, CMMI-1825189, and CMMI-1937984, as well as Pacific Earthquake Engineering Research Center (PEER) Grant 1132-NCTRBM and US Geological Survey (USGS) Award G18AP-00006. This support is gratefully acknowledged, as well as access to the NZGD. The authors also appreciate the comments by the anonymous reviewers, which resulted in improvements in the paper. However, any opinions, findings, and conclusions or recommendations expressed in this paper are those of the authors and do not necessarily reflect the views of NSF, PEER, USGS, NZGD, or the anonymous reviewers.

Supplemental Materials

Table S1 is available online in the ASCE Library (www.ascelibrary.org).

References

Allen, J., et al. 2010. "Geotechnical reconnaissance of the 2010 Darfield (Canterbury) earthquake." *Bull. N. Z. Soc. Earthquake Eng.* 43 (4): 243–320. https://doi.org/10.5459/bnzsee.43.4.243-320.

Baise, L. G., R. B. Higgins, and C. M. Brankman. 2006. "Liquefaction hazard mapping-statistical and spatial characterization of susceptible units." *J. Geotech. Geoenviron. Eng.* 132 (6): 705–715. https://doi.org/10.1061/(ASCE)1090-0241(2006)132:6(705).

Boulanger, R. W., and I. M. Idriss. 2012. "Probabilistic standard penetration test-based liquefaction-triggering procedure." *J. Geotech. Geoenviron. Eng.* 138 (10): 1185–1195. https://doi.org/10.1061/(ASCE)GT.1943-5606.0000700.

Boulanger, R. W., and I. M. Idriss. 2014. *CPT and SPT based liquefaction triggering procedures*. Rep. No. UCD/CGM-14/01. Davis, CA: Center for Geotechnical Modelling, Dept. of Civil and Environmental Engineering, UC Davis, CA.

Bradley, B. A. 2013. "A New Zealand-specific pseudo-spectral acceleration ground-motion prediction equation for active shallow crustal earthquakes based on foreign models." *Bull. Seismol. Soc. Am.* 103 (3): 1801–1822. https://doi.org/10.1785/0120120021.

Bradley, B. A. 2014. "Site-specific and spatially-distributed ground-motion intensity estimation in the 2010–2011 Canterbury earthquakes." *Soil Dyn. Earthquake Eng.* 61–62 (Jun–Jul): 83–91. https://doi.org/10.1016/j.soildyn.2014.01.025.

Cetin, K. O., A. Der Kiureghian, and R. B. Seed. 2002. "Probabilistic models for the initiation of seismic soil liquefaction." *Struct. Saf.* 24 (1): 67–82. https://doi.org/10.1016/S0167-4730(02)00036-X.

Cetin, K. O., R. B. Seed, A. Der Kiureghian, K. Tokimatsu, L. F. R. E. HarderKayen Jr., R. E. Kayen, and R. E. S. Moss. 2004. "Standard penetration test-based probabilistic and deterministic assessment of seismic soil liquefaction potential." *J. Geotech. Geoenviron. Eng.* 130 (12): 1314–1340. https://doi.org/10.1061/(ASCE)1090-0241(2004)130:12(1314).

Cetin, K. O., R. B. Seed, R. E. Kayen, R. E. S. Moss, H. T. Bilge, M. Ilgac, and K. Chowdhury. 2018. "SPT-based probabilistic and deterministic assessment of seismic soil liquefaction triggering hazard." *Soil Dyn. Earthquake Eng.* 115 (Dec): 698–709. https://doi.org/10.1016/j.soildyn.2018.09.012.

Chung, J., and J. D. Rogers. 2017. "Deterministic and probabilistic assessment of liquefaction hazards using the liquefaction potential index and liquefaction reduction number." *J. Geotech. Geoenviron. Eng.* 143 (10): 0401703. https://doi.org/10.1061/(ASCE)GT.1943-5606.0001772.

Cramer, C. H., G. J. Rix, and K. Tucker. 2008. "Probabilistic liquefaction hazard maps for Memphis, Tennessee." *Seismol. Res. Lett.* 79 (3): 416–423. https://doi.org/10.1785/gssrl.79.3.416.

Cubrinovski, M., J. D. Bray, M. Taylor, S. Giorgini, B. Bradley, L. Wotherspoon, and J. Zupan. 2011. "Soil liquefaction effects in the central business district during the February 2011 Christchurch earthquake." *Seismol. Res. Lett.* 82 (6): 893–904. https://doi.org/10.1785/gssrl.82.6.893.

Cubrinovski, M., A. Rhodes, N. Ntritsos, and S. Van Ballegooy. 2019. "System response of liquefiable deposits." *Soil Dyn. Earthquake Eng.* 124 (Sep): 212–229. https://doi.org/10.1016/j.soildyn.2018.05.013.

Dixit, J., D. M. Dewaikar, and R. S. Jangid. 2012. "Assessment of liquefaction potential index for Mumbai City." *Nat. Hazards Earth Syst. Sci.* 12 (9): 2759–2768. https://doi.org/10.5194/nhess-12-2759-2012.

Dobry, R. 1989. "Some basic aspects of soil liquefaction during earthquakes." In Vol. 558 of *Earthquake hazards and the design of constructed facilities in the eastern United States*, edited by K. H. Jacob and C. J. Turkstra, 172–182. New York: Annals of the New York Academy of Sciences.

Fawcett, T. 2006. "An introduction to ROC analysis." *Pattern Recognit. Lett.* 27 (8): 861–874. https://doi.org/10.1016/j.patrec.2005.10.010.

Geyin, M., A. J. Baird, B. W. Maurer. 2020. "Field assessment of liquefaction prediction models based on geotechnical versus geospatial data, with lessons for each." *Earthquake Spectra* 36 (3): 1386–1411. https://doi.org/10.1177/8755293019899951.

Geyin, M., B. W. Maurer, B. A. Bradley, R. A. Green, and S. van Ballegooy. 2021. "CPT-based liquefaction case histories compiled from three earthquakes in Canterbury, New Zealand." *Earthquake Spectra* 37 (4): 2920–2945. https://doi.org/10.1177/8755293021996367.

Green, R. A., J. J. Bommer, A. Rodriguez-Marek, B. W. Maurer, P. Stafford, B. Edwards, P. P. Kruiver, G. de Lange, and J. van Elk. 2019. "Addressing limitations in existing 'simplified' liquefaction triggering evaluation procedures: Application to induced seismicity in the Groningen gas field." *Bull. Earthquake Eng.* 17 (8): 4539–4557. https://doi.org/10.1007/s10518-018-0489-3.

Green, R. A., J. J. Bommer, A. Rodriguez-Marek, and P. J. Stafford. 2016. *Unbiased cyclic resistance ratio relationships for evaluating liquefaction potential in Groningen*, edited by J. van Elk and D. Doornhof, 61. Groningen, Netherlands: Nederlandse Aardolie Maatschappij B.V.

Green, R. A., A. Bradshaw, and C. D. P. Baxter. 2022. "Accounting for intrinsic soil properties and state variables on liquefaction triggering in simplified procedures." *J. Geotech. Geoenviron. Eng.* 148 (7): 04022056. https://doi.org/10.1061/(ASCE)GT.1943-5606.0002823.

Green, R. A., M. Cubrinovski, B. Cox, C. Wood, L. Wotherspoon, B. Bradley, and B. W. Maurer. 2014. "Select liquefaction case histories from the 2010-2011 Canterbury earthquake sequence." *Earthquake Spectra* 30 (1): 131–153. https://doi.org/10.1193/030713EQS066M.

Green, R. A., and S. M. Olson. 2015. "Interpretation of liquefaction field case histories for use in developing liquefaction triggering curves." In *Proc., 6th Int. Conf. on Earthquake Geotechnical Engineering (6ICEGE)*. Christchurch, New Zealand. London: International Society of Soil Mechanics and Geotechnical Engineering.

Green, R. A., S. Upadhyaya, C. M. Wood, B. W. Maurer, B. R. Cox, L. Wotherspoon, B. A. Bradley, and M. Cubrinovski. 2017. "Relative efficacy of CPT- versus V_S-based simplified liquefaction evaluation procedures." In *Proc., 19th Int. Conf. on Soil Mechanics and Geotechnical Engineering*. London: International Society of Soil Mechanics and Geotechnical Engineering.

Green, R. A., C. Wood, B. Cox, M. Cubrinovski, L. Wotherspoon, B. Bradley, T. Algie, J. Allen, A. Bradshaw, and G. Rix. 2011. "Use of DCP and SASW tests to evaluate liquefaction potential: Predictions vs. observations during the recent New Zealand earthquakes." *Seismol. Res. Lett.* 82 (6): 927–938. https://doi.org/10.1785/gssrl.82.6.927.

Hayati, H., and R. D. Andrus. 2008. "Liquefaction potential map of Charleston, South Carolina based on the 1986 earthquake." *J. Geotech. Geoenviron. Eng.* 134 (6): 815–828. https://doi.org/10.1061/(ASCE)1090-0241(2008)134:6(815).

Holzer, T. L. 2008. "Probabilistic liquefaction hazard mapping." In *Geotechnical Earthquake Engineering and Soil Dynamics IV*, ASCE Geotechnical Special Publication 181, edited by D. Zeng, M. T. Manzari, and D. R. Hiltunen. Reston, VA: ASCE.

Holzer, T. L., M. J. Bennett, T. E. Noce, A. C. Padovani, and J. C. Tinsley III. 2006. "Liquefaction hazard mapping with LPI in the greater

Oakland, California, area." *Earthquake Spectra* 22 (3): 693–708. https://doi.org/10.1193/1.2218591.

Holzer, T. L., T. E. Noce, and M. J. Bennett. 2009. "Scenario liquefaction hazard maps of Santa Clara Valley, Northern California." *Bull. Seismol. Soc. Am.* 99 (1): 367–381. https://doi.org/10.1785/0120080227.

Idriss, I. M., and R. W. Boulanger. 2008. *Soil liquefaction during earthquakes*. Monograph MNO-12. Oakland, CA: Earthquake Engineering Research Institute.

Idriss, I. M., and R. W. Boulanger. 2010. *SPT-based liquefaction triggering procedures*. Rep. No. UCD/CGM-10, 2. Davis, CA: Univ. of California at Davis.

Ishihara, K. 1985. "Stability of natural deposits during earthquakes." In Vol. 1 of *Proc., 11th Int. Conf. on Soil Mechanics and Foundation Engineering*, 321–376. Rotterdam, Netherlands: A.A. Balkema.

Ishihara, K., and M. Yoshimine. 1992. "Evaluation of settlements in sand deposits following liquefaction during earthquakes." *Soils Found.* 32 (1): 173–188. https://doi.org/10.3208/sandf1972.32.173.

Iwasaki, T., F. Tatsuoka, K. Tokida, and S. Yasuda. 1978. "A practical method for assessing soil liquefaction potential based on case studies at various sites in Japan." In *Proc., 2nd Int. Conf. on Microzonation*, 885–896. Washington, DC: National Science Foundation.

Juang, C. H., T. Jiang, and R. D. Andrus. 2002. "Assessing probability-based methods for liquefaction potential evaluation." *J. Geotech. Geoenviron. Eng.* 128 (7): 580–589. https://doi.org/10.1061/(ASCE)1090-0241(2002)128:7(580).

Juang, C. H., C. Ou, C. Lu, and Z. Luo. 2010. "Probabilistic framework for assessing liquefaction hazard at a given site in a specified exposure time using standard penetration testing." *Can. Geotech. J.* 47 (6): 674–687. https://doi.org/10.1139/T09-127.

Kayen, R., R. Moss, E. Thompson, R. Seed, K. Cetin, A. Kiureghian, Y. Tanaka, and K. Tokimatsu. 2013. "Shear-wave velocity–based probabilistic and deterministic assessment of seismic soil liquefaction potential." *J. Geotech. Geoenviron. Eng.* 139 (3): 407–419. https://doi.org/10.1061/(ASCE)GT.1943-5606.0000743.

Maurer, B. W., R. A. Green, M. Cubrinovski, and B. Bradley. 2015a. "Assessment of CPT-based methods for liquefaction evaluation in a liquefaction potential index framework." *Géotechnique* 65 (5): 328–336. https://doi.org/10.1680/geot.SIP.15.P.007.

Maurer, B. W., R. A. Green, M. Cubrinovski, and B. Bradley. 2015b. "Calibrating the liquefaction severity number (LSN) for varying misprediction economies: A case Study in Christchurch, New Zealand." In *Proc., 6th Int. Conf. on Earthquake Geotechnical Engineering*. London: International Society of Soil Mechanics and Geotechnical Engineering.

Maurer, B. W., R. A. Green, M. Cubrinovski, and B. Bradley. 2015c. "Fines-content effects on liquefaction hazard evaluation for infrastructure in Christchurch, New Zealand." *Soil Dyn. Earthquake Eng.* 76 (Sep): 58–68. https://doi.org/10.1016/j.soildyn.2014.10.028.

Maurer, B. W., R. A. Green, M. Cubrinovski, and B. A. Bradley. 2014. "Evaluation of the liquefaction potential index for assessing liquefaction hazard in Christchurch, New Zealand." *J. Geotech. Geoenviron. Eng.* 140 (7): 04014032. https://doi.org/10.1061/(ASCE)GT.1943-5606.0001117.

Maurer, B. W., R. A. Green, and O. S. Taylor. 2015d. "Moving towards an improved index for assessing liquefaction hazard: Lessons from historical data." *Soils Found.* 55 (4): 778–787. https://doi.org/10.1016/j.sandf.2015.06.010.

Maurer, B. W., R. A. Green, S. van Ballegooy, B. A. Bradley, and S. Upadhyaya. 2017a. "Performance comparison of probabilistic and deterministic liquefaction triggering models for hazard assessment in 23 global earthquakes." In *Geo-Risk 2017: Reliability-Based Design and Code Developments*, ASCE Geotechnical Special Publication 283, edited by J. Huang, G. A. Fenton, L. Zhang, and D. V. Griffiths, 31–42. Reston, VA: ASCE.

Maurer, B. W., R. A. Green, S. van Ballegooy, and L. Wotherspoon. 2017b. "Assessing liquefaction susceptibility using the CPT soil behavior type index." In *Proc., 3rd Int. Conf. on Performance-Based Design in Earthquake Geotechnical Engineering (PBDIII)*. London: International Society of Soil Mechanics and Geotechnical Engineering.

Maurer, B. W., R. A. Green, S. van Ballegooy, and L. Wotherspoon. 2019. "Development of region-specific soil behavior type index correlations for evaluating liquefaction hazard in Christchurch, New Zealand." *Soil Dyn. Earthquake Eng.* 117 (Feb): 96–105. https://doi.org/10.1016/j.soildyn.2018.04.059.

Moss, R. E. S., R. B. Seed, R. E. Kayen, J. P. Stewart, A. Der Kiureghian, and K. O. Cetin. 2006. "CPT-based probabilistic and deterministic assessment of in situ seismic soil liquefaction potential." *J. Geotech. Geoenviron. Eng.* 132 (8): 1032–1051. https://doi.org/10.1061/(ASCE)1090-0241(2006)132:8(1032).

NZGD (New Zealand Earthquake Commission). 2016. "New Zealand geotechnical database." Accessed August 24, 2016. https://www.nzgd.org.nz/Default.aspx.

Oommen, T., L. G. Baise, and R. Vogel. 2010. "Validation and application of empirical liquefaction models." *J. Geotech. Geoenviron. Eng.* 136 (12): 1618–1633. https://doi.org/10.1061/(ASCE)GT.1943-5606.0000395.

Papathanassiou, G. 2008. "LPI-based approach for calibrating the severity of liquefaction-induced failures and for assessing the probability of liquefaction surface evidence." *Eng. Geol.* 96 (1–2): 94–104. https://doi.org/10.1016/j.enggeo.2007.10.005.

Papathanassiou, G., A. Mantovani, G. Tarabusi, D. Rapti, and R. Caputo. 2015. "Assessment of liquefaction potential for two liquefaction prone areas considering the May 20, 2012 Emilia (Italy) earthquake." *Eng. Geol.* 189 (Apr): 1–16. https://doi.org/10.1016/j.enggeo.2015.02.002.

Papathanassiou, G., S. Pavlides, and A. Ganas. 2005. "The 2003 Lefkada earthquake: Field observation and preliminary microzonation map based on liquefaction potential index for the town of Lefkada." *Eng. Geol.* 82 (1): 12–31. https://doi.org/10.1016/j.enggeo.2005.08.006.

Robertson, P. K., and C. E. Wride. 1998. "Evaluating cyclic liquefaction potential using cone penetration test." *Can. Geotech. J.* 35 (3): 442–459. https://doi.org/10.1139/t98-017.

Sana, H., and S. K. Nath. 2016. "Liquefaction potential analysis of the Kashmir valley alluvium, NW Himalaya." *Soil Dyn. Earthquake Eng.* 85 (Jun): 11–18. https://doi.org/10.1016/j.soildyn.2016.03.009.

Seed, H. B., and I. M. Idriss. 1971. "Simplified procedure for evaluating soil liquefaction potential." *J. Soil Mech. Found. Div.* 97 (9): 1249–1273. https://doi.org/10.1061/JSFEAQ.0001662.

Sönmez, H. 2003. "Modification of the liquefaction potential index and liquefaction severity mapping for a liquefaction-prone area (Inegol, Turkey)." *Eng. Geol.* 44 (7): 862–871. https://doi.org/10.1007/s00254-003-0831-0.

Ulmer, K. J. 2019. "Development of an energy-based liquefaction evaluation procedure." Dissertation submitted in partial fulfillment of a Ph.D., Dept. of Civil and Environmental Engineering, Virginia Tech.

Ulmer, K. J., R. A. Green, and A. Rodriguez-Marek. 2022. "Recommended b-value for Computing Number of Equivalent Cycles and Magnitude Scaling Factors for Simplified Liquefaction Triggering Evaluation Procedures." *J. Geotech. Geoenviron. Eng.* 148 (12): 04022113. https://doi.org/10.1061/(ASCE)GT.1943-5606.0002926.

Upadhyaya, S., R. A. Green, B. W. Maurer, and A. Rodriguez-Marek. 2019a. "Selecting factor of safety against liquefaction for design based on cost considerations." In *Proc., 7th Int. Conf. on Earthquake Geotechnical Engineering*. London: International Society of Soil Mechanics and Geotechnical Engineering.

Upadhyaya, S., R. A. Green, B. W. Maurer, A. Rodriguez-Marek, and S. van Ballegooy. 2022a. "Limitations of surface liquefaction manifestation severity index models used in conjunction with simplified stress-based triggering models." *J. Geotech. Geoenviron. Eng.* 148 (3): 04021194. https://doi.org/10.1061/(ASCE)GT.1943-5606.0002725.

Upadhyaya, S., R. A. Green, A. Rodriguez-Marek, B. W. Maurer, L. Wotherspoon, B. A. Bradley, and M. Cubrinovski. 2019b. "Influence of corrections to recorded peak ground accelerations due to liquefaction on predicted liquefaction response during the M_w 6.2, February 2011 Christchurch earthquake." In *Proc., 13th Australia New Zealand Conf. on Geomechanics 2019*. Gap, QLD, Australia: Australian Geomechanics Society.

Upadhyaya, S., B. W. Maurer, R. A. Green, and A. Rodriguez-Marek. 2018. "Effect of non-liquefiable high fines-content, high plasticity soils on liquefaction potential index (LPI) performance." In *Geotechnical*

Earthquake Engineering and Soil Dynamics V: Liquefaction Triggering, Consequences, and Mitigation, ASCE Geotechnical Special Publication 290, edited by S. J. Brandenberg and M. T. Manzari, 191–198. Reston, VA: ASCE.

Upadhyaya, S., B. W. Maurer, R. A. Green, and A. Rodriguez-Marek. 2021. "Selecting the optimal factor of safety or probability of liquefaction triggering for engineering projects based on misprediction costs." *J. Geotech. Geoenviron. Eng.* 147 (6): 04021026. https://doi.org/10.1061/(ASCE)GT.1943-5606.0002511.

Upadhyaya, S., B. W. Maurer, R. A. Green, A. Rodriguez-Marek, and S. van Ballegooy. 2022b. "Surficial liquefaction manifestation severity thresholds for profiles having high fines-content, high plasticity soils." *Can. Geotech. J.* https://doi.org/10.1139/cgj-2022-0092.

van Ballegooy, S., S. C. Cox, C. Thurlow, H. K. Rutter, T. Reynolds, G. Harrington, J. Fraser, and T. Smith. 2014a. *Median water table elevation in Christchurch and surrounding area after the 4 September 2010 Darfield earthquake: Version 2*. GNS Science Rep. No. 2014/18. Lower Hutt, New Zealand: GNS.

van Ballegooy, S., R. A. Green, J. Lees, F. Wentz, and B. W. Maurer. 2015. "Assessment of various CPT based liquefaction severity index frameworks relative to the Ishihara (1985) H_1–H_2 boundary curves." *Soil Dyn. Earthquake Eng.* 79 (Dec): 347–364. https://doi.org/10.1016/j.soildyn.2015.08.015.

van Ballegooy, S., P. Malan, V. Lacrosse, M. E. Jacka, M. Cubrinovski, J. D. Bray, T. D. O'Rourke, S. A. Crawford, and H. Cowan. 2014b. "Assessment of liquefaction-induced land damage for residential Christchurch." *Earthquake Spectra* 30 (1): 31–55. https://doi.org/10.1193/031813EQS070M.

van Ballegooy, S., P. J. Malan, M. E. Jacka, V. I. M. F. Lacrosse, J. R. Leeves, J. E. Lyth, and H. Cowan. 2012. "Methods for characterising effects of liquefaction in terms of damage severity." In *Proc., 15th World Conf. on Earthquake Engineering (15 WCEE)*. Tokyo: International Association for Earthquake Engineering.

Whitman, R. V. 1971. "Resistance of soil to liquefaction and settlement." *Soils Found.* 11 (4): 59–68. https://doi.org/10.3208/sandf1960.11.4_59.

Wotherspoon, L. M., R. P. Orense, B. A. Bradley, B. R. Cox, C. Wood, and R. A. Green. 2014. *Geotechnical characterisation of Christchurch strong motion stations*. Earthquake Commission Biennial Grant Rep., Project No. 12/629. Wellington, New Zealand: New Zealand Earthquake Commission.

Wotherspoon, L. M., R. P. Orense, R. A. Green, B. A. Bradley, B. R. Cox, and C. M. Wood. 2015. "Assessment of liquefaction evaluation procedures and severity index frameworks at Christchurch strong motion stations." *Soil Dyn. Earthquake Eng.* 79 (Dec): 335–346. https://doi.org/10.1016/j.soildyn.2015.03.022.

Yalcin, A., C. Gokceoglu, and H. Sönmez. 2008. "Liquefaction severity map for Aksaray city center (Central Anatolia, Turkey)." *Nat. Hazards Earth Syst. Sci.* 8 (4): 641–649. https://doi.org/10.5194/nhess-8-641-2008.

Youd, T. L., and M. J. Bennett. 1983. "Liquefaction sites imperial Valley, California." *J. Geotech. Eng.* 109 (3): 440–457. https://doi.org/10.1061/(ASCE)0733-9410(1983)109:3(440).

Zhang, G., P. K. Robertson, and R. W. I. Brachman. 2002. "Estimating liquefaction-induced ground settlements from CPT for level ground." *Can. Geotech. J.* 39 (5): 1168–1180. https://doi.org/10.1139/t02-047.

Zhu, J., L. G. Baise, and E. M. Thompson. 2017. "An updated geospatial liquefaction model for global application." *Bull. Seismol. Soc. Am.* 107 (3): 1365–1385. https://doi.org/10.1785/0120160198.

Zou, K. H. 2007. "Receiver operating characteristic (ROC) literature research." Accessed March 10, 2016. https://www.spl.harvard.edu/archive/spl-pre2007/pages/ppl/zou/roc.html.